**HEFAT2012**
**9th International Conference on Heat Transfer, Fluid Mechanics and Thermodynamics**
**16 – 18 July 2012**
**Malta**

# MODELLING OF PULSED AIR JET IMPINGEMENT HEAT TRANSFER IN A SINGLE-PHASE AND GAS-DROPLETS MIST JET

Pakhomov M.A. and Terekhov V.I.*
*Author for correspondence
Laboratory of Thermal and Gas Dynamics,
Kutateladze Institute of Thermophysics, Siberian Branch of Russian Academy of Sciences
Novosibirsk, 630090,
Russia,
E-mail: terekhov@itp.nsc.ru

## ABSTRACT

The flow structure and heat transfer of an intermittent impinging single-phase air and water mist jet with low mass fraction of droplets (not more than 1 %) is studied numerically. In the range of small distances between the tube edge and obstacle $H/(2R) \le 6$ in the pulsed jet heat transfer at stagnation point increases with a rise of pulse frequency, whereas at high distances $H/(2R) > 8$ frequency rise causes heat transfer reduction. Heat transfer intensity during flow pulse action increases and exceeds significantly the corresponding value for the stationary case. When there is no flow, the value of Nusselt number decreases considerably. Results obtained were compared with available data of other authors, and satisfactory agreement was obtained for the influence of pulse frequency on heat transfer of the gas jet with impinging surface.

## INTRODUCTION

Impinging jet is employed in many industrial applications (for example drying of sheets of various materials, cooling of electronic devices and GT blades, printing processes, etc) due to heat and mass transfer enhancement around of stagnation point [1].

An addition of evaporating droplets causes a significant increase in heat transfer intensity in comparison with the single-phase flow. In many technical applications intermittent (pulsed) flow occurs due to moving parts, by vibrations or flow oscillations. Studies performed show a complex physical situation that in some cases leads to significant heat transfer enhancement, however, also decrease of heat transfer can occur [2–4]. The impingement of pulsed mist flow on hot surfaces also occurs in practical situations, which require a comprehensive knowledge of the flow patterns and the interaction of the spray with the impinging surface. Pulsed spray impingement on hot surfaces has capability of removing large amounts of heat due to use of the latent heat of evaporation [5,6]. An increase in heat transfer can change from 10 to 100% in vicinity of the stagnation point and to 40-50% in the zone of wall jet. A decrease in heat transfer varies within 10-30% over the whole impinging surface.

The aim of the present work is numerical simulation of the effect of droplets evaporation on the flow and heat transfer in turbulent impinging pulsed jets.

## NOMENCLATURE

| | | |
|---|---|---|
| $d$ | [m] | Droplet diameter |
| DC | [-] | The time of duty cycle of the flow |
| ER | [-] | Heat transfer enhancement ratio |
| $f$ | [Hz] | Frequency of the pulses |
| $H$ | [m] | Distance between pipe exit cross-section and impinging flat plate |
| $H/(2R)$ | [-] | Dimensionless distance between pipe exit and impinging flat plate |
| Nu | [-] | Nusslt number, Nu = $\alpha 2R/\lambda$ |
| $q_W$ | [W/m$^2$] | Heat flux density |
| $2R$ | [m] | Pipe diameter |
| $M_{L1}$ | [-] | Initial droplets mass fraction |
| $U_i$ | [m/s] | Components of the mean velocity |
| Re | [-] | Reynolds number, $2RU_{m1}/\nu$ |
| $r$ | [m] | Radial coordinate |
| $St_d$ | [-] | Strouhal number, $St_d = f2R/U_{m1}$ |
| $T$ | [K] | Temperature |
| $T_i$ | [s] | Time of pulses |
| $We_W$ | [-] | Weber number, based on the wall conditions |
| $t$ | [s] | Time |
| $t_c$ | [s] | time cycle |
| $t_{off}$ | [s] | Off-time pulse cycle |
| $t_{on}$ | [s] | On-time pulse cycle |
| $x$ | [m] | Axial coordinate |
| $y$ | [m] | Distance normal to the wall |
| $y_+$ | [m] | Dimensionless distance from the wall |

Special characters

| | | |
|---|---|---|
| $\sigma$ | [N/m] | Surface tension |

Subscripts

| | |
|---|---|
| $L$ | Dispersed phase |
| $ns$ | Pulsed impinging jet (non-steady) |

| | |
|---|---|
| *st* | Steady-state jet |
| *W* | Parameter on the wall condition |
| 0 | Parameter under conditions at the stagnation point |
| 1 | Parameter under initial conditions |

## GOVERNING EQUATIONS

The motion of the gas-droplets impinging jet consisting of an incompressible viscous flow and small droplets is considered. The droplet behavior in a turbulent fluid and their back action on the flow is determined by the drag, gravity force, turbulent transport and turbulent diffusion, while the forces due to associated with displaced masses and the Basset force can be neglected. In order to account for the interaction between phases, i.e. momentum exchange and heat and mass transfer, the conservation equations have to be extended by appropriate source/sink terms.

Flow dynamics and heat transfer in the impinging pulsed gas-droplets jet were obtained with the use of the Eulerian approach initially developed [7] for description of turbulent flows with solid particles without heat transfer between the phases. For the gas phase we used the set of non-steady-state RANS equations. In the study is considered for the gas phase the second moment closure by [7]. For the dispersed phase velocity fluctuations were used kinetic stresses equations, turbulent heat flux and temperature fluctuations equations by [8]. The two-way coupling model was used along with the particulate feedback onto the mean distribution of the gas phase.

In the Eulerian formulation, the dispersed solid phase is treated as the second continuous fluid. The governing equations of particle motion have the similar differential form to fluid flow equations and separate boundary conditions are applied to each phase. The most noteworthy advantage of the Eulerian scheme is that the solution to the equations of motion yields average flow conditions, such as particle concentration and velocity, in each computational cell. The Eulerian model is computationally more efficient compared with its Lagrangian counterpart. The interaction between phases (coupling) is easily considered in Eulerian models by the addition of extra terms in the relevant equations. Moreover, the numerical procedures utilized to solve the fluid phase equations can also be applied to the solid phase.

The main assumption of the work is the particles deposited on the wall from the two-phase flow momentarily evaporate, leaving the wall surface always dry. This assumption is quite valid for heated surface and used if the difference between wall temperature $T_W$ and droplet temperature $T_{WL}$ is $T_W - T_{WL} \geq 40$. The mass concentration of particles decreases in the downstream direction due to their deposition onto the plate surface and due to wall jet expansion. The droplet temperature is assumed to be uniform over the droplet radius and droplets are considered as spherical. The volume concentration of the dispersed phase $\Phi < 10^{-4}$ is assumed to be sufficiently small so inter-particle collisions can be neglected and the initial droplet diameter being $d_1 \leq 100$ μm. No coalescence occurs in the flow because the amount of the dispersed phase is small, and droplets never undergo brake-up. Weber number, based on the wall conditions $\mathrm{We}_W = \rho_W \left|\vec{U}_L\right|^2 d_W / \sigma_W < 1$ whereas the critical Weber number according to the data reported in [10] is $\mathrm{We}_* = 7$.

## NUMERICAL REALIZATION

Numerical solution is obtained by the method of finite volumes at staggered grid. For convective terms of differential equation s the QUICK procedure is used. For differential flows central differences are applied. The pressure field is corrected by the finite-volumetric agreed SIMPLEC procedure. Third-order upwind discretization scheme for the convective terms and second-order central difference for diffusion terms are used.

Computational domain is a cylinder with a size of $20R$ in a radial direction and height of $H$. The computational grid nonuniform both in axial and radial directions is applied. Fine grids are used near impinging surface, jet axis and the pipe exit cross-section. At least 10 control volumes (CVs) have been generated to be able to resolve the mean velocity field and turbulent quantities in the viscosity-affected near-wall region ($y_+ < 10$). Grid sensitivity studies have been carried out to determine the optimum grid resolution that gives a mesh independent solution. All predictions are carried out on the grid with 200×256 CVs in axial and radial directions. Computations on the grid with 300×400 CVs are carried out additionally. The solutions presented here were considered grid independent.

The results of preliminary calculations for a single-phase flow in the pipe with the length of $150R$ are used for the gas phase velocity and turbulence on the pipe edge. This is enough to achieve a fully developed turbulent gas flow. The symmetry conditions are set on the jet axis for gas and dispersed phases. The no-slip conditions are set on the wall for the gas phase. Boundary conditions on the outer border of jet and impinging surface for dispersed phase correspond to the conditions of "absorbing surface" [11], when droplets do not return to the flow after the contact with wall or external border. On outer edge of the computational domain (the wall jet periphery) the conditions $\partial\phi / \partial r = 0$ for the all variables are set. The components of Reynolds stresses are determined at the same points on the control volume surface as the corresponding components of averaged gas velocities by the method of [8].

## VALIDATION ANALYSIS FOR THE SINGLE-PHASE AIR STEADY-STATE IMPINGING JET

For comparative analysis in the case of single-phase steady-state air jet were used experimental data on flow [12] and heat transfer of the impinging air jet [13].

## NUMERICAL RESULTS AND DISCUSSIONS

All computations are carried out for the single-phase air and gas-droplets mist impinging jets under the atmospheric pressure. The schematic of the impinging jet development is shown in the Figure 1.

The pipe diameter is $2R$ = 20 mm. The mean velocity of the gas flow on the axis of the pipe exit cross-section is $U_{m1}$ = 20 m/s, Reynolds number for the gas phase is Re = $2RU_{m1}/\nu$ = $2.6\times10^4$. The dispersed phase is given as uniform distribution of parameters over the cross-section on the pipe edge. The initial velocity of dispersed phase is $U_{L1} = 0.8U_{m1}$. The initial size of droplets varies within $d_1$ = 0–100 μm, and its mass concentration varies within $M_{L1}$ = 0–1 %. The wall temperature is $T_W$ = 373 K, and initial gas and droplets temperatures are $T_1$ = $T_{L1}$ = 293 K. The distance between the pipe edge and target surface changes within $H/(2R)$ = 1–10.

Frequency of pulsed flow was $f$ = 0–60 Hz. The time of duty cycle of the flow DC was determined by the formula: $\mathrm{DC} = t_{on}/t_c = t_{on}/(t_{on}+t_{off})$, where $t_{on}$ is time, when the flow is available, and $t_{off}$ is time, when there is no flow (see Figure 2). In this study DC = 0.5 and we used in the computations only the rectangular form of the pulse. The Strouhal number, determined by the tube diameter, is $\mathrm{St}_d = f2R/U_{m1} = 5\times10^{-4}$–0.1 and Strouhal number, calculated by the distance to the obstacle surface, is $\mathrm{St}_H = fH/U_{m1} = 6\times10^{-4}$–3.5. This Strouhal number $\mathrm{St}_H$ shows how many times the gas flow reaches the plate surface during the cycle. All numerical simulations were performed for the rectangular shape of the intermittency both for the single-phase and mist impinging jets, and equal flow rates for the steady-state and pulsed impinging jets.

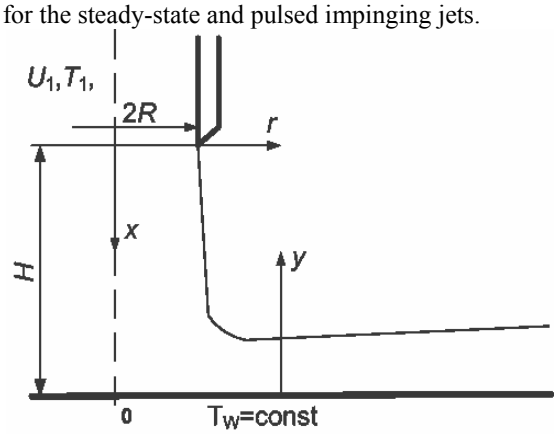


**Figure 1** The schematic of the impinging jet development

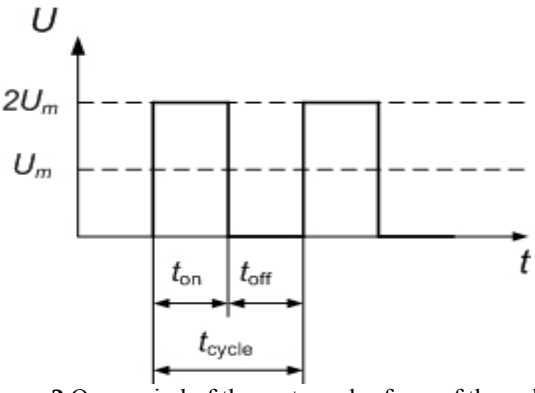


**Figure 2** One period of the rectangular form of the pulse

**Single-Phase Pulsed Impinging Jet**

Profiles of velocity (blue line) and Nusselt number in stagnation point $\mathrm{Nu}_0 = \alpha_0 2R/\lambda$ (red lines) are given in the Figure 3 for the distances to the barrier $H/(2R)$ = 2 and 6, where $\alpha_0$ is the heat transfer coefficient in the stagnation point. The heat transfer in stagnation point for the steady-state impinging jet are depicted with horizontal lines *3* and *4* for the distances to the barrier $H/(2R)$ = 2 and 6, respectively (dashed red lines). Five cycles were chosen as the time of presentation in the given diagram. The Nusselt number $\mathrm{Nu}_0$ number change in time has harmonic character. At that local maxima and minima of heat transfer are located respectively in the end of gas phase flow cycle and in the moment before the start of new impulse. It should be noted that at the impulse frequency ($f$ = 5 Hz) minimal value of heat emission is not reduced to null magnitude but is approximately half of the maximal value. This proves the inertial properties of the impinging jet and the boundary layer formed on the surface.

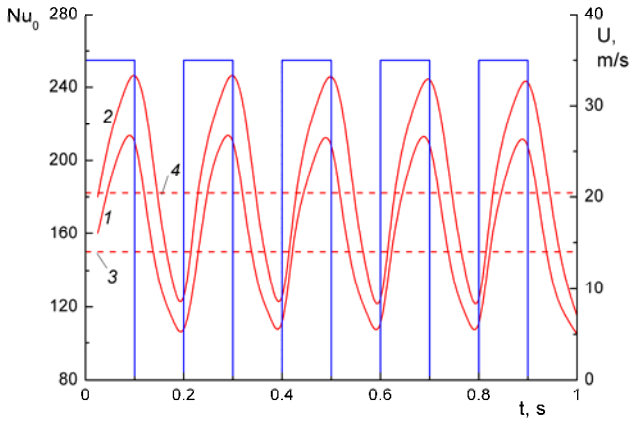


**Figure 3** The heat transfer in the stagnation point and velocity as a function of time for $H/(2R)$ = 2 and 6, Re = 23000, $T_W$ = 373 K, $T_1$ = 293 K, $f$ = 5 Hz, $U_1$ = 35 м/с, DC = 0.5, $\mathrm{St}_d$ = $2.85\times10^{-3}$. *1* – $H/(2R)$ = 2, *2* – 6.

The effect of Reynolds number on averaged heat transfer in stagnation point in the intermittent impinging jet at its different frequencies is demonstrated in the Fig. 4. Five cycles were chosen as time of presentation in the given diagram. The line *1* here complies with steady-state jet. Since straight lines was obtained in the log–log diagram, it is seen that $\mathrm{Nu}_0 \sim \mathrm{Re}^m$. The exponent $m$ = 0.57. It is noted that in [13], the exponent $m$ = 0.5 was derived. However, when the influence of a parameter, i.e. the Reynolds number, is studied, it is more reasonable to consider sets of experimental data separately. This guarantees that the only influence factor on the results is the examined variation of the studied parameter. The value of exponent $m$ was varied in several experimental and numerical papers in the diapason $m$ = 0.5–0.68 [14].

As it is apparent at the studied in the paper impulse frequencies heat transfer in pulsed jet is higher than in the steady-state one. The increase of Reynolds number leads to that the effect of heat transfer intensification decreases and data for all frequencies approach to the value for one-phase impinging jet. Similar result should be expected for other distances between the nozzle and the barrier; however this very interesting effect requires more detailed investigation.

In the Figure 5 there are results of comparison of our calculations and measurements [3] for the single-phase jet. Experiments were performed for axisymmetric jet at Re = 7500, $St_d = 2.4\times10^{-3}$–$7.6\times10^{-2}$, $q_W = 420$ W/m$^2$, $H/(2R) = 3$ and $t_{on} = t_{off}$. Flow parameters in the pipe exit cross-section were set on the basis of preliminary calculation in the pipe with $2R = 15$ mm diameter and $40R$ length.

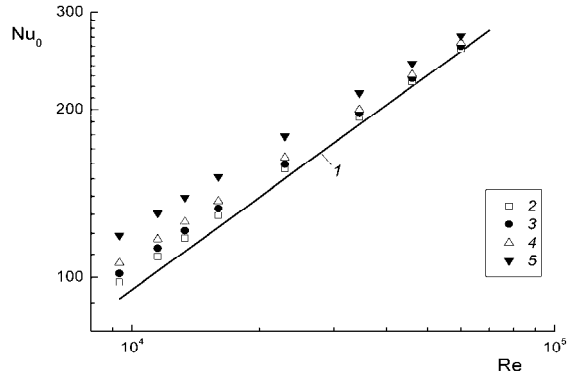


**Figure 4** The heat transfer in the stagnation point as a function of Reynolds number at $H/(2R) = 2$. *1* – steady-state impinging jet ($f = 0$ Hz), 2 – 5 our numerical results: *2* – $f = 5$ Гц , *3* – 10, *4* – 20, *5* – 60.

In the Figure 5 is shown the distribution of enhancement ratio $ER = Nu_{0,ns} / Nu_{0,st}$ on the radial coordinate. Here $Nu_{0,ns}$ is Nusselt number in the intermittent impinging jet and $Nu_{0,st}$ is heat transfer in the steady-state impinging jet. The time averaged Nusselt number was determined from relationship $\mathrm{Nu} = \frac{1}{TC}\int_0^{TC} \mathrm{Nu}(r,t)dt$ and $TC$ is the period of time (minimum five time cycles). Open and closed points are the measurements by [3].

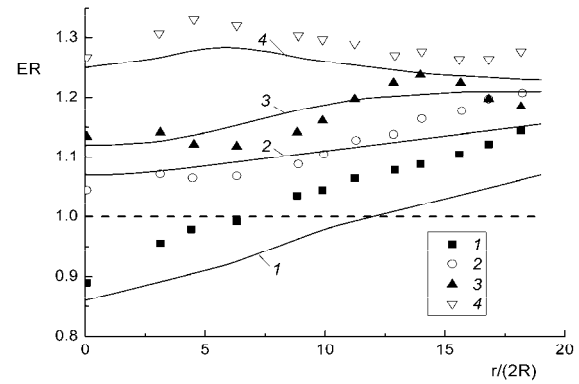


**Figure 5** Radial distribution of the enhancement ratio ER in the stagnation point along radial coordinate at various frequencies. Points are the measurements by [3], lines are the author's computations. *1* – $f = 1.25$ Hz, *2* – 5, *3* – 10, *4* – 40.

The increase of distance between pipe exit cross-section and impinging surface leads to the noticeably increase of heat transfer value in the stagnation point pulsed jet for small frequencies ($f \le 5$ Hz) compared with the steady-state jet. For the frequency at $f = 1.25$ Hz approximately in half a length of the calculated area heat transfer suppression is observed. This is specific both for experiments and our predictions.

The effect of impulse frequency on heat transfer in the stagnation point is given in the Fig. 6. Symbols are experiments of [3]. Initially in the area of small frequencies ($f < 5$ Hz) heat transfer suppression is observed; at further increase of $f$ the specific is heat transfer intensification ($ER > 1.2$ at $f = 40$ Hz). It may be pointed out that the results of our numerical calculations fairly correlate with the experiments [3] in the entire area of the studied frequencies *f*.

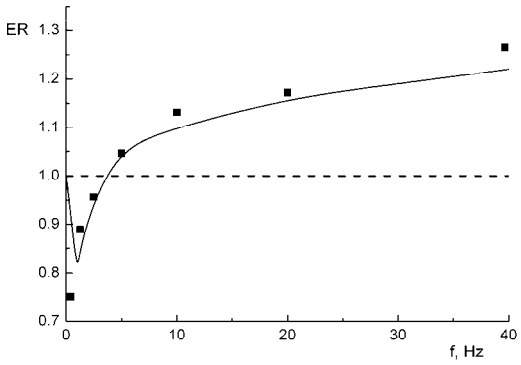


**Figure 6** Distribution of heat transfer enhancement ratio in the stagnation point as a function of pulses frequencies. Points are the measurements [3], curve is the author's simulations.

**Gas-Droplets Mist Pulsed Intermittent Impinging Jet**

The second part of the paper was devoted to the numerical simulations of flow and heat transfer in the pulsed mist impinging jet.

Figure 8 shows the effect of pulses frequency on the heat transfer rate along the target surface for $H/(2R) = 2$ (a) и 6. The time averaged local Nusselt number increases with frequency and Strouhal number. The heat transfer in the pulsed jet exceeds the corresponding value for the steady-state jet impingement in the case for relatively low spacing $H/(2R) = 2$ (see Figure 8a) and it is lower than that one for the large distance $H/(2R) = 6$ (see Figure 8b). The main regularities of the heat transfer behavior in the two-phase intermittent impinging jet are correlated with the regularities of heat transfer in the steady-state jet impingement [1,13].

The time averaged heat transfer in stagnation point at varying distance between the pipe exit cross-section and flat surface for different impulse frequencies are presented in the Figure 9. Mass gas flow rate in pulsed and steady-state impinging jets for the data presented in the Figure 9 remained unchanged and Reynolds number $\mathrm{Re} = 2.3\times10^4$. Dashed lines are the prediction for steady-state mist jet impingement at $M_{L1} = 0.01$. Heat transfer simulation in this case was performed on the steady-state equations of the model.

Note main peculiarities of the influence of flow pulsation on heat transfer in stagnation point. Maximal value of heat transfer in the frontal point both for the steady-state and pulsed jets is observed at the distance $H/(2R) \approx 6$. This distance approximately complies with the length of potential core of the jet and such regularity for the steady mode is mentioned in numerous works [1,13,14]. The character of heat transfer change depending on the distance between pipe exit and impinging surface in pulsed jet in comparison with steady-state jet remains unchanged. It was obtained for pulsed impinging jet that at $H/(2R) \le 5$ an increase in frequency of pulses leads to the heat transfer enhancement around the stagnation point. In the range of distances $5 \le H/(2R) \le 6$, as it is apparent in the Figure 9, it is not the effect of jet pulsation on the heat transfer. For large distance $H/(2R) > 6$ the increase frequency leads to heat transfer suppression in the stagnation zone. These findings are consistent with the results in the Figure 8. Heat transfer augmentation is found to be up to 30% in comparison with the steady-state mist jet.

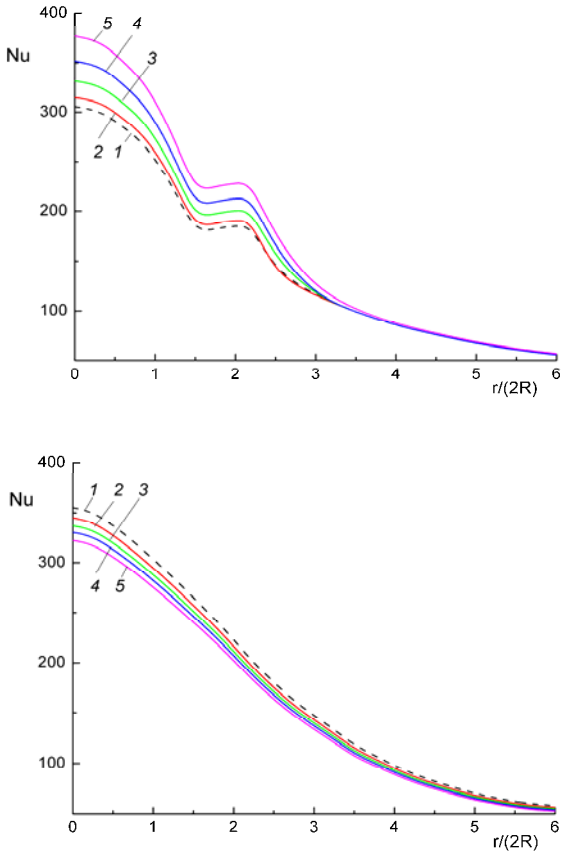


**Figure 8** The effect of pulses frequency on the time averaged local heat transfer at $H/(2R) = 2$ (a) и 6 (b). Re = 23000, $d_1$ = 50 μm, $M_{L1}$=0.01. *1* – $f$ = 0 Hz (steady-state jet); *2* – 5; *3* – 10; *4* – 30; *5* – 60.

The comparison between our predictions and experiments for pulsed mist jet measurements was provided. These results are presented in the Figure 10. Here $\alpha$ is the heat transfer coefficient and $J$ is the mass flow rate of the mist flow. Agreement between our computation results and measurements data of [6] was rather good especially for the small value of the time of the pulse $T_i$ (line *1*) when the wall surface in the experiments is dry. The increase of $T_i$ leads to the formation of liquid film and spots on target plate (observed in the measurements) and the residual between our simulations and experiments is rise (line *2*). We did not take into account the film formation on the wall from deposited droplets. We assumed droplets deposited onto the impinging surface momentarily evaporate (solid curves). The predictions without taking into account the heat spend the droplets heat up and evaporation $q_{WL}$ (dashed curve) agreed better with measurements.

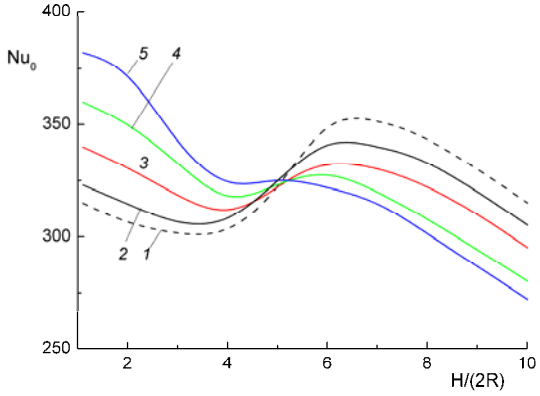


**Figure 9** Heat transfer in the stagnation point vs various distance between pipe exit and plate surface. Re = $2.3\times10^4$, $d_1$ = 50 μm, $M_{L1}$= 0.01, $f$ = 5 Hz, $t_{on}$= $t_{off}$. *1* – $f$ = 0 Hz (steady-state jet); *2* – 5; *3* – 10, *4* – 30; *5* – 60.

## CONCLUSIONS

The numerical simulation of the single-phase air and gas-droplets mist impinging jets in the paper was provided.

The effect of droplets evaporation on the flow and heat transfer in turbulent impinging pulsed jet for the low droplets mass fraction ($M_{L1} \le 1$ %) was performed. The numerical model was based on the Eulerian approach. In this study was used the Second Moment Closure by Craft and Launder by [8] for computations of the gas phase turbulence. For the dispersed phase velocity fluctuations the kinetic stresses equations, turbulent heat flux and temperature fluctuations equations were modelled with the use of Zaichik model of [9]. The two-way coupling model was used along with the particulate feedback onto the mean distribution of the gas phase.

In the range of small distances between the tube edge and obstacle $H/(2R) \le 6$ in the pulsed jet heat transfer at stagnation point increases with a rise of pulse frequency, whereas at high distances $H/(2R) > 8$ frequency rise causes heat transfer reduction. Heat transfer intensity during flow pulse action increases and exceeds significantly the corresponding value for the stationary case. At time moment, when there is no flow, the value of Nusselt number decreases considerably. Results obtained were compared with published data of other authors, and satisfactory agreement was obtained for the influence of

pulse frequency on heat transfer of the gas jet with impinging surface.

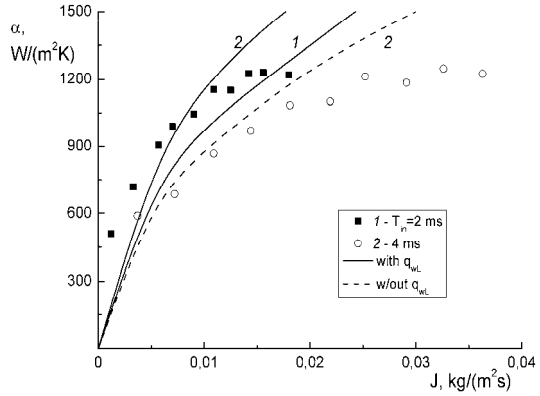


**Figure 10** Heat transfer coefficient in pulsed mist impinging jet. Symbols are experimental results, curves are computations. $H = 230$ mm, $f = 1 – 50$ Hz, $T = T_\infty = 295$ K, $T_W = 373$ K, $U_{L1} = 14.8$ m/s. *1* – $T_i = 2$ ms, *2* – 4.


## ACKNOWLEDGEMENTS

This work was partially supported by the Russian Foundation for Basic Research (Projects No. 12-08-00504) and by the Programme of Department of Energetic, Mechanics and Control Processes of Russian Academy of Sciences (Project No. 10-2).


## REFERENCES


[1] Martin K., Heat and mass transfer between impinging gas jets and solid surfaces, *Advances in Heat Transfer*, Vol. 13, 1977, pp. 1-60.

[2] Zumbrunnen D.A. and Aziz M., Convective heat transfer enhancement due to intermittency in an impinging jet, *ASME Journal of Heat Transfer*, Vol. 115, 1993, pp. 91-98.

[3] Middelberg G. and Herwig H., Convective heat transfer under unsteady impinging jets: the effect of the shape of the unsteadiness, *Heat Mass Transfer*, Vol. 45, 2009, pp. 1519-1532.

[4] Xu P., Yu B., Qiu S.X., Poh H.J. and Mujumdar A.S, Turbulent impinging jet heat transfer enhancement due to intermittent pulsation, *International Journal of Thermal Sciences*, Vol. 49, 2010, pp. 1247-1252.

[5] Moreira A.L.N., and Panao M.R.O., Heat transfer at multiple-intermittent impact of a hollow cone spray, *International Journal of Heat and Mass Transfer*, Vol. 49, 2006, pp. 4132-4151.

[6] Nazarov A.D., Serov A.F., and Bodrov M.V., Intensification of cooling by a pulsed gas-droplet flow: Equipment, parameters, and results, *Technical Physics*, Vol. 55, 2010, pp. 724-727.

[7] Derevich I.V., and Zaichik L.I., Particle deposition from a turbulent flow, *Fluid Dynamics*, Vol. 23, 1988, pp. 722-729.

[8] Craft T.J., and Launder B.E., New wall-reflection model applied to the turbulent impinging jet, *AIAA Journal*, Vol. 30, 1992, pp 2970-2972.

[9] Zaichik L.I., A statistical model of particle transport and heat transfer in turbulent shear flows, *Physics of Fluids*, Vol. 11, 1999, pp. 1521-1534.

[10] Mastanaiah K., and Ganic E.N., Heat transfer in two-component dispersed flow, *ASME Journal of Heat Transfer*, Vol. 103, 1981, pp. 300-306.

[11] Derevich I.V., The hydrodynamics and heat transfer and mass transfer of particles under conditions of turbulent flow of gas suspension in a pipe and in an axisymmetric jet, *High Temperature*, Vol. 40, 2002, pp. 78-91.

[12] Cooper D., Jackson D.C., Launder B.E., and Liao G.X., Impinging jet studies for turbulence model assessment – I. Flow field experiments, *International Journal of Heat and Mass Transfer*, Vol. 36, 1993, pp. 2675-2584.

[13] Behnia M., Parneix S., Shabany Y., and Durbin P.A., Numerical study of turbulent heat transfer in confined and unconfined impinging jets, *International Journal of Heat and Fluid Flow*, Vol. 20, 1999, pp. 1–9.

[14] Jambunathan K., Lai E., Moss M.A., and Button B.L., A review of heat transfer data for single circular jet impingement, *International Journal of Heat and Fluid Flow*, Vol. 13, 1992, pp. 106-115.